IEEE Access
Multidisciplinary | Rapid Review | Open Access Journal

Received November 8, 2020, accepted December 7, 2020, date of publication December 22, 2020, date of current version January 4, 2021.

Digital Object Identifier 10.1109/ACCESS.2020.3046616

Magnetic Integrated LLC Resonant Converter Based on Independent Inductance Winding

SHENGWEI GAO AND ZIYI ZHAO
Tianjin Key Laboratory of Advanced Technology of Electrical Engineering and Energy, Tiangong University, Tianjin 300387, China
School of Electrical Engineering and Automation, Tiangong University, Tianjin 300387, China

Corresponding author: Ziyi Zhao (zzy674110028@126.com)

This work was supported in part by the National Natural Science Foundation of China (NSFC) under Grant 51807139, in part by the Science and Technology Planning Project of Tianjin under Grant 20YDTPJC01520, and in part by the Graduate Research and Innovation Project of Tianjin under Grant 2019YJSS026.

ABSTRACT LLC resonant converter has the advantages of high frequency and high efficiency, and has been developed rapidly and widely used in recent years. However, due to the presence of multiple magnetic components in the circuit, the improvement of power density is limited. To solve this problem, integrated magnetic transformer is usually designed to replace the discrete magnetics. While, the leakage inductance of the transformer cannot be controlled, the loss of the converter increases. In this paper, a magnetic integrated LLC resonant converter with independent inductance winding is proposed. The resonant inductance and magnetizing inductance are integrated with the transformer in the same magnetic core by using the decoupling integration method. Compared with the existing solution of magnetic integrated LLC resonant converter, this method can reduce the leakage inductance between the transformer windings and decrease the magnetic saturation of the integrated magnetics, thereby reducing the magnetic core loss and improving the efficiency of the converter. Compared with the discrete magnetics, the volume and weight of the magnetic components are reduced by 25.68% and 43.82% respectively, making the power density of the converter effectively improved. Finally, an experimental prototype of integrated magnetic LLC resonant converter with operating frequency of 350kHz and output power of 400W is built. The experimental results verify the correctness of the design scheme.

INDEX TERMS LLC resonant converter, independent inductance winding, integrated magnetics, equivalent model, finite element simulation analysis, efficiency.

I. INTRODUCTION

With the continuous development of DC power supply, the operation modes of the traditional hard switching PWM converter cannot meet people's needs. As shown in figure 1, due to the advantages of wide range voltage input, wide gain range, high transmission efficiency and easy realization of soft-switching, LLC resonant converter has developed rapidly in recent years, and its application fields are also constantly expanding [1]–[6]. Although the LLC resonant converter achieves Zero Voltage Switching (ZVS) for the primary-side switches and Zero Current Switching (ZCS) for the secondary-side rectifier diodes in full load range [7], [8]. However, with the increase of switching frequency, the loss of the converter is also increasing. At the same time, the volume and weight of the converter are increased due to the multiple magnetic components involved in the resonant circuit, which is not conducive to the improvement of power density. In order to solve this problem, Magnetic Integration Technology can be used to integrate multiple discrete magnetics (DM) in the converter, which can effectively reduce the volume, weight, cost, and loss of magnetic components, so as to improve the power density of the converter [9]–[11].

In recent years, comprehensive studies on the design of resonant parameters, DC gain analysis, soft switching realization conditions, control methods and strategies have been carried out [12]–[15]. Due to the inherent easy magnetic integration characteristics of LLC resonant converter, the leakage inductance of the transformer is used to replace the resonant inductance, and the magnetic columns of the transformer is opened the air gap to construct the magnetizing inductance. Past researches on the integrated

The associate editor coordinating the review of this manuscript and approving it for publication was Yijie Wang.

magnetics (IM) has mostly used EE type magnetic core structure. The difference lies in the coil winding method and the air gap setting. In reference [16], a general structure model of EE core IM with four coils was proposed. The circuit structure was analyzed by using the magnetic circuit-electric circuit dual transformation method. The IM structure suitable for LLC resonant converters was obtained by designing the air gap and coil arrangement. Reference [17] applied IM to three-level full bridge LLC resonant converter, which optimized the selection of IM parameters, reduced the transformer secondary side leakage inductance, and realized soft- switching in full load range. Reference [18] used IM in a three-phase LLC resonant converter, replacing three discrete transformers with a single magnetic core trans-former. The proposed structure reduced the generation of unbalanced output current. In reference [19], to solve the problem that the transformer leakage inductance was insufficient and unable to provide the required resonant inductance, the magnetic shunt was introduced into the IM to make the winding structure produce enough resonant inductance. The relationship between transformer leakage inductance and magnetic shunt characteristics was investi-gated, the modeling and design methods were given. In reference [20], EI magnetic core was used to design the distribution of transformer windings, and a half-turn planar transformer structure with integrated leakage inductance was proposed, which used its terminal effect to introduce a filter to reduce the output voltage ripple.

Although the above methods reduce the volume and improve the power density of the converter, there are still shortcomings in the stability of the magnetic components structure, the control of magnetic saturation, the leakage inductance control, and the converter conversion efficiency. In this paper, a magnetic integrated LLC resonant converter with independent inductance winding was proposed. The resonant inductance and magnetizing inductance are inte-grated with transformer in the same core by using the decoupling integration method. The variation of IM magnetic flux in different working modes of the converter was analyzed and the optimization design formulas were derived. The finite element model of the magnetic components were established to verify the distribution of magnetic flux density and magnetic field in different magnetic components. Finally, an experimental prototype of magnetic integrated LLC resonant converter with switch-ing frequency of 350kHz and output power of 400W is built to verify the correctness of the design scheme.

II. MAGNETIC INTEGRATED METHODS FOR LLC RESONANT CONVERTER

A. INTEGRATED MAGNETIC TRANSFORMER

LLC resonant converter contains three magnetic components: resonant inductance, magnetizing inductance and transformer. A transformer with air gap is used to integrate the magnetizing inductance and transformer. The resonant

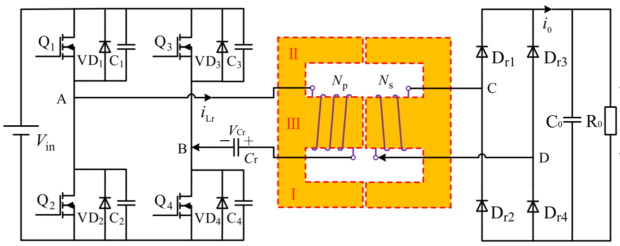

FIGURE 1. Integrated magnetic transformer structure.

inductance is achieved by adjusting the distance between the primary and secondary windings of the transformer to produce leakage inductance. In this way, one transformer can get all the magnetics needed, which effectively improves the power density of the converter.

However, this design has the following disadvantages: First is that the leakage inductance of the IM transformer cannot be accurately controlled during the design and manufacture; Then, the leakage inductance of the trans-former is usually small, resulting in the converter operating in a limited frequency range, thus limiting the input voltage range; Finally, since the leakage inductance exists not only on the transformer primary side but also on the secondary side, the leakage inductance of the transformer secondary side will affect the withstand voltage of the rectifier diode, thereby increasing the on-state loss of the rectifier diode.

B. RESONANT INDUCTANCE AND TRANSFORMER DECOUPLING INTEGRATION

In order not to affect the original working mode and to improve the power density of the converter, the resonant inductance and the transformer should be decoupled and integrated.

The resonant inductance and transformer integrated structure of LLC resonant converter and its equivalent magnetic circuit are shown in figure 2 and figure 3 respectively. In order to make rational use of the magnetic core, the resonant inductance is wound on the two side columns of the magnetic core, and the transformer is wound on the middle column of the magnetic core. The same air gap is opened for the three columns of the magnetic core.

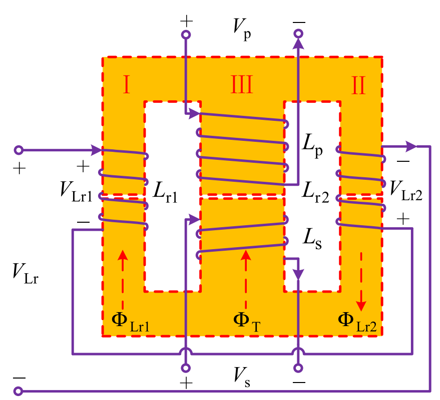

FIGURE 2. IM structure of resonant inductance and transformer.

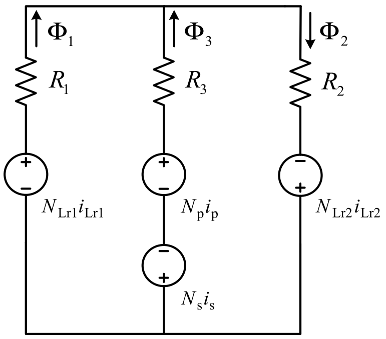

FIGURE 3. **IM equivalent magnetic circuit.**

Figure 2 is the IM structure diagram. The transformer includes the primary winding and the secondary winding, which are wound on the magnetic column III. L_p and L_s are the self-inductance generated by the primary winding and the secondary winding respectively; the resonant induct-ance L_r is divided into two parts, L_{r1} and L_{r2}, which are respectively wound on the magnetic columns I and II; Φ_T, $\Phi_{Lr1}$and Φ_{Lr2} represent the magnetic flux generated by the transformer winding, inductance L_{r1} and inductance L_{r2} respectively; V_p, V_s , $V_{Lr1}$and V_{Lr2} represent the voltage of the transformer primary winding, the secondary winding, the inductance $L_{r1}$and the inductance L_{r2} respectively. Figure 3 shows the equivalent magnetic circuit of IM. R_1, $R_2$and R_3 represent the magnetic resistance on the magnetic columns I, II and III respectively; N_p and N_s represent the primary winding turns and the secondary winding turns of the transformer respec-tively; N_{Lr1} and N_{Lr2} represent the winding turns of induc-tance L_{r1} and inductance L_{r2} respect-ively; i_p, i_s , i_{Lr1} and i_{Lr2} represent the current of the transformer primary winding, the secondary winding, the inductance $L_{r1}$and the induc-tance L_{r2} respectively; N_pi_p and N_si_s are Magnetomotive Force of the transformer primary winding and secondary winding; $N_{Lr1}i_{Lr1}$ and $N_{Lr2}i_{Lr2}$ are Magnetomotive Force of resonant inductance on both side columns; Φ_1, Φ_2 and Φ_3 are the magnetic fluxes produced by windings under the joint action of the columns I, II and III of the magnetic core respectively.

C. ANALYSIS OF IM ELECTRIC CIRCUIT - MAGNETIC CIRCUIT COUPLING PRINCIPLE

To facilitate design and not affect the structure of the mag-netic core, the three columns of magnetic core are open the same air gaps at the same time. Combining figure 2 with the IM winding structure model and according to the Ohm's law of the magnetic circuit, the magnetic flux generated by each winding is:

$$\begin{cases} \Phi_{Lr1} = \dfrac{N_{Lr1}i_{Lr1}}{R_1+R_2//R_3} = \dfrac{N_{Lr1}i_{Lr1}(R_2+R_3)}{\Delta} \\ \Phi_{Lr2} = \dfrac{N_{Lr2}i_{Lr2}}{R_2+R_1//R_3} = \dfrac{N_{Lr2}i_{Lr2}(R_1+R_3)}{\Delta} \\ \Phi_T = \dfrac{N_pi_p-N_si_s}{R_3+R_1//R_2} = \dfrac{(N_pi_p-N_si_s)(R_1+R_2)}{\Delta} \end{cases} \tag{1}$$

Among them, $\Delta = R_1R_2 + R_1R_3 + R_2R_3$. According to the IM equivalent magnetic circuit in figure 3, the mag-netic fluxes generated by each winding under the joint action of the columns I, II and III of magnetic core are:

$$\begin{cases} \Phi_1 = \Phi_{Lr1} + \Phi_{Lr2}\dfrac{R_3}{R_1+R_3} - \Phi_T\dfrac{R_2}{R_1+R_2} \\ \Phi_2 = \Phi_{Lr1}\dfrac{R_3}{R_2+R_3} + \Phi_{Lr2} + \Phi_T\dfrac{R_1}{R_1+R_2} \\ \Phi_3 = -\Phi_{Lr1}\dfrac{R_2}{R_2+R_3} + \Phi_{Lr2}\dfrac{R_1}{R_1+R_3} + \Phi_T \end{cases} \tag{2}$$

Substituting equation (1) into equation (2) acquires equa-tion (3):

$$\begin{cases} \Phi_1 = N_{Lr1}i_{Lr1}\dfrac{R_2+R_3}{\Delta} + N_{Lr2}i_{Lr2}\dfrac{R_3}{\Delta} \\ \qquad - (N_pi_p - N_si_s)\dfrac{R_2}{\Delta} \\ \Phi_2 = N_{Lr1}i_{Lr1}\dfrac{R_3}{\Delta} + N_{Lr2}i_{Lr2}\dfrac{R_1+R_3}{\Delta} \\ \qquad + (N_pi_p - N_si_s)\dfrac{R_1}{\Delta} \\ \Phi_3 = -N_{Lr1}i_{Lr1}\dfrac{R_2}{\Delta} + N_{Lr2}i_{Lr2}\dfrac{R_1}{\Delta} \\ \qquad + (N_pi_p - N_si_s)\dfrac{R_1+R_2}{\Delta} \end{cases} \tag{3}$$

Since the resonant inductance voltage $V_{Lr} = V_{Lr1} + V_{Lr2}$, and the resonant inductance current $i_{Lr} = i_{Lr1} = i_{Lr2}$, so according to Faraday's law of electromagnetic induction, the transformer primary winding voltage V_p, the se-condary winding voltage $V_s$and the resonant induc-tance voltage V_{Lr} can be respectively expressed as follows:

$$\begin{cases} V_p = N_p\dfrac{d\Phi_3}{dt} \\ V_s = -N_s\dfrac{d\Phi_3}{dt} \\ V_{Lr} = V_{Lr1} + V_{Lr2} \\ = N_{Lr1}\dfrac{d\Phi_1}{dt} + N_{Lr2}\dfrac{d\Phi_2}{dt} \end{cases} \tag{4}$$

According to equation (1) to (4), the relationship between the winding voltage and current of the IM can be obtained:

$$\begin{bmatrix} V_{Lr} \\ V_p \\ V_s \end{bmatrix} = \begin{bmatrix} L_r & M_{pLr} & M_{sLr} \\ M_{pLr} & L_p & -M_{ps} \\ M_{sLr} & -M_{ps} & L_s \end{bmatrix} \begin{bmatrix} \dfrac{di_{Lr}}{dt} \\ \dfrac{di_p}{dt} \\ \dfrac{di_s}{dt} \end{bmatrix} \tag{5}$$

Among them, M_{pLr} represents the mutual induct-ance between the transformer primary winding and the reso-nant inductance L_r; M_{sLr} represents the mutual inductance between the transformer secondary winding and the resonant inductance L_r; and M_{ps} represents the mutual inductance between the transformer primary winding and secondary winding.

$$\begin{cases} M_{\mathrm{pLr}} = \dfrac{N_{\mathrm{p}}(N_{\mathrm{Lr2}}R_1 - N_{\mathrm{Lr1}}R_2)}{\Delta} \\ M_{\mathrm{sLr}} = \dfrac{N_{\mathrm{s}}(N_{\mathrm{Lr1}}R_2 - N_{\mathrm{Lr2}}R_1)}{\Delta} \\ M_{\mathrm{ps}} = \dfrac{N_{\mathrm{p}}N_{\mathrm{s}}(R_1 + R_2)}{\Delta} \\ L_{\mathrm{p}} = \dfrac{N_{\mathrm{p}}^2(R_1 + R_2)}{\Delta} \\ L_{\mathrm{s}} = \dfrac{N_{\mathrm{s}}^2(R_1 + R_2)}{\Delta} \\ L_{\mathrm{r}} = \dfrac{N_{\mathrm{Lr1}}^2(R_2 + R_3) + N_{\mathrm{Lr2}}^2(R_1 + R_3)}{\Delta} \\ \qquad + \dfrac{2N_{\mathrm{Lr1}}N_{\mathrm{Lr2}}R_3}{\Delta} \end{cases} \tag{6}$$

From equation (5) and equation (6), the coupling coefficient can be obtained as follows:

$$\begin{cases} K_{\mathrm{ps}} = \dfrac{-M_{\mathrm{ps}}}{\sqrt{L_{\mathrm{p}}L_{\mathrm{s}}}} = -1 \\ K_{\mathrm{pLr}} = \dfrac{M_{\mathrm{pLr}}}{\sqrt{L_{\mathrm{r}}L_{\mathrm{p}}}} \\ K_{\mathrm{sLr}} = \dfrac{M_{\mathrm{sLr}}}{\sqrt{L_{\mathrm{r}}L_{\mathrm{s}}}} \end{cases} \tag{7}$$

Among them, K_{ps} is the coupling coefficient between the transformer primary winding and the secondary winding; K_{pLr} is the coupling coefficient between the transformer primary winding and the resonant inductance; and K_{sLr} is the coupling coefficient between the transformer secondary winding and the resonant inductance.

It can be seen from the above equations that the coupling coefficients K_{pLr} and K_{sLr} of the resonant inductance and the transformer can be adjusted by the number of turns of the resonant inductance on both sides of the magnetic core. According to equation (6) and equation (7), when the winding mode of resonant inductance is: $N_{\mathrm{Lr1}}/R_1 = N_{\mathrm{Lr2}}/R_2$, that's to say, to satisfy:

$$N_{\mathrm{Lr2}}R_1 = N_{\mathrm{Lr1}}R_2 \tag{8}$$

Bring equation (8) into equation (6), the mutual inductance between the transformer winding and the resonant inductance is $M_{\mathrm{pLr}} = M_{\mathrm{sLr}} = 0$, and the coupling coefficients $K_{\mathrm{pLr}} = K_{\mathrm{sLr}} = 0$.

Through the above analysis, the magnetic flux generated by the resonant inductance on both sides of the magnetic core will not affect the center column transformer. Similarly, the magnetic flux generated by the center column transformer will not affect the side column resonant inductance. In this way, the magnetic circuit between the windings will not interplay, and the resonant inductance and the transformer can be completely decoupled.

III. ANALYSIS AND DESIGN OF IM

A. ANALYSIS OF MAGNETIC INTEGRATED LLC RESONANT CONVERTER

For the magnetic integrated LLC resonant converter, it is necessary to ensure that the constant switching frequency

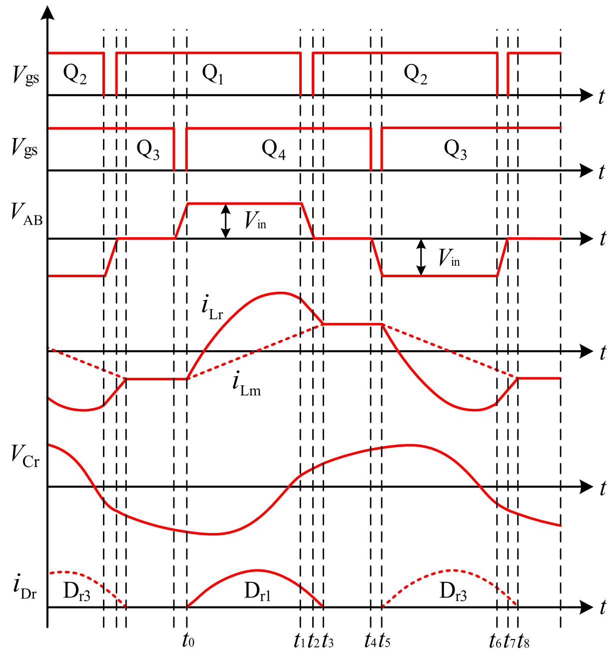

FIGURE 4. The main waveform of the converter under phase-shift control.

keeps the converter in a high efficiency working state. Therefore, the constant frequency control is adopted to make the switching frequency equal to the resonant frequency, which ensures that the converter always works at the highest efficiency point. Moreover, the constant frequency control is easy to optimize the design of magnetic components and improve the power density of the converter. Therefore, the constant frequency phase-shift control is adopted in this paper.

The waveform of LLC resonant converter under the phase-shift control are shown in figure 4. Among them, V_{AB} is the voltage between primary side full bridge; $V_{\mathrm{Cr}}$is the voltage of the resonant capacitance; i_{Dr} is the current of the rectifier diode; i_{Lr} and i_{Lm} represent the current of the resonant inductance L_{r} and the magnetizing inductance L_{m} respectively. Figure 5 shows the IM operation mode of the LLC resonant converter. Figure 6 illustrates the equivalent AC magnetic circuit diagram of the IM, where R_1, R_2 and R_3 are the equivalent magnetic resistance of the magnetic columns respectively. According to Faraday's law of electromagnetic induction, the AC magnetic flux of each magnetic columns are determined by the volt-second product of the winding, and the AC equivalent power of each magnetic columns are $\Phi_{\mathrm{AC1}}(\mathrm{t})$, $\Phi_{\mathrm{AC2}}(\mathrm{t})$ and $\Phi_{\mathrm{AC3}}(\mathrm{t})$.

1) MODE A [t_0-t_1]

At t_0, Q_1 and Q_4 are turned on, the voltage V_{AB} at points A and B is equal to V_{in}, and the transformer secondary rectifier diodes D_{r1} and D_{r4} are turned on, clamp-ing the transformer primary side voltage at nV_0, and i_{Lm} increases linearly. At this stage, L_{r} and C_{r} resonate together, and the expressions of V_{Cr},

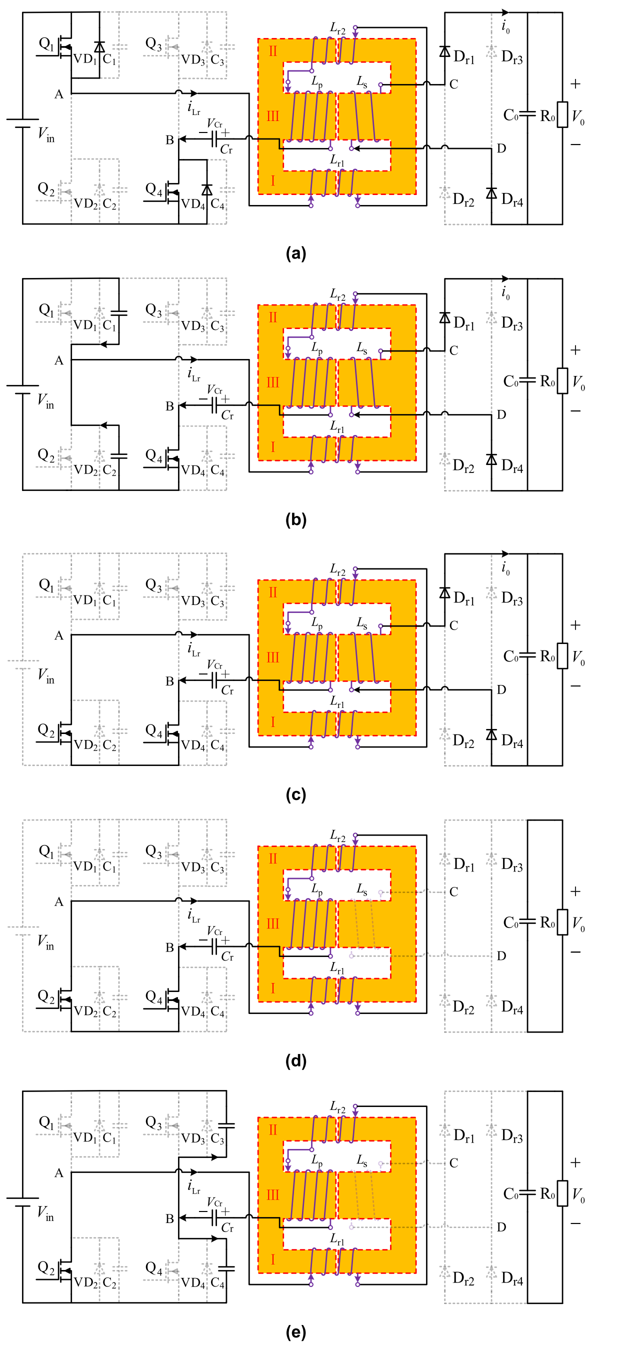

FIGURE 5. IM operation mode of LLC resonant converter. (a) Mode a $[t_0\text{-}t_1]$. (b) Mode b $[t_1\text{-}t_2]$. (c) Mode c $[t_2\text{-}t_3]$. (d) Mode d $[t_3\text{-}t_4]$. (e) Mode e $[t_4\text{-}t_5]$.

i_{Lr} and i_{Lm} are as follows:

$$\begin{cases} V_{\mathrm{Cr}}(t)=(V_{\mathrm{in}}-nV_0)-[(V_{\mathrm{in}}-nV_0)-V_{\mathrm{Cr}}(t_0)]cos\omega(t-t_0) \\ \qquad +I_{\mathrm{Lr}}(t_0)Z_{\mathrm{r}}\sin\omega_{\mathrm{r}}(t-t_0) \\ i_{\mathrm{Lr}}(t)=[(V_{\mathrm{in}}-nV_0)-V_{\mathrm{Cr}}(t_0)]\dfrac{1}{Z_{\mathrm{r}}}\sin\omega_{\mathrm{r}}(t-t_0) \\ \qquad +I_{\mathrm{Lr}}(t_0)\cos\omega(t-t_0) \\ i_{\mathrm{Lm}}(t)=I_{\mathrm{Lr}}(t_0)+\dfrac{nV_0}{L_{\mathrm{m}}}(t-t_0) \end{cases} \tag{9}$$

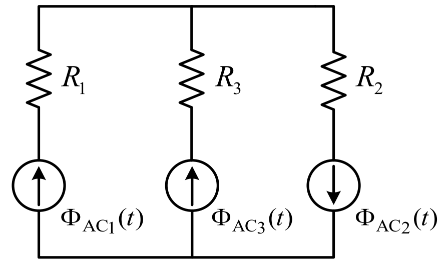

FIGURE 6. Equivalent AC magnetic circuit.

In this equation, ω_{r} is the resonant angular frequency of the resonant inductance and the resonant capacitance, and Z_{r} is the characteristic impedance.

At this stage, the magnetic flux expression of the side columns and the center column of the core are as follows:

$$\begin{cases} \Phi_{\mathrm{AC1}}(t)=\Phi_{\mathrm{AC2}}(t)=\dfrac{V_{\mathrm{in}}-nV_0-V_{\mathrm{Cr}}}{N_{\mathrm{Lr}}}(t-t_0) \\ \Phi_{\mathrm{AC3}}(t)=(\dfrac{nV_0}{N_{\mathrm{P}}}-\dfrac{V_0}{N_{\mathrm{s}}})(t-t_0) \end{cases} \tag{10}$$

2) MODE B $[t_1\text{-}t_2]$

At t_1, Q_1 is turned off and Q_4 is still on. The energy stored in the resonant inductance L_r charges the parasitic capacitance C_1 of Q_1 and discharges the parasitic capacitance C_2 of Q_2. Due to the buffering effect of C_1, Q_1 is turned off at zero voltage, and the transformer secondary rectifier diodes D_{r1} and D_{r4} are still on.

At this stage, the magnetic flux expression of the side column and the center column of the core are as follows:

$$\begin{cases} \Phi_{\mathrm{AC1}}(t)=\Phi_{\mathrm{AC2}}(t)=\dfrac{V_{\mathrm{AB}}-nV_0-V_{\mathrm{Cr}}}{N_{Lr}}(t-t_1) \\ \Phi_{\mathrm{AC3}}(t)=(\dfrac{nV_0}{N_{\mathrm{P}}}-\dfrac{V_0}{N_{\mathrm{s}}})(t-t_1) \end{cases} \tag{11}$$

3) MODE C $[t_2\text{-}t_3]$

At t_2, the parasitic capacitance C_1 rises to V_{in}, the voltage of C_2 drops to zero, Q_2 turns on at zero voltage, and Q_4 is still on. At this time, V_{AB} is zero, the transformer secondary rectifier diodes D_{r1} and D_{r4} are still on, and the transformer primary side voltage is still clamped at nV_0. The expressions of V_{Cr}, i_{Lr} and i_{Lm} are as follows:

$$\begin{cases} V_{\mathrm{Cr}}(t)=-nV_0-[-nV_0-V_{\mathrm{Cr}}(t_2)]cos\omega(t-t_2) \\ \qquad +I_{\mathrm{Lr}}(t_2)Z_{\mathrm{r}}\sin\omega_{\mathrm{r}}(t-t_2) \\ i_{\mathrm{Lr}}(t)=[-nV_0-V_{\mathrm{Cr}}(t_2)]\dfrac{1}{Z_{\mathrm{r}}}\sin\omega_{\mathrm{r}}(t-t_2) \\ \qquad +I_{\mathrm{Lr}}(t_2)\cos\omega(t-t_2) \\ i_{\mathrm{Lm}}(t)=I_{\mathrm{Lr}}(t_2)+\dfrac{nV_0}{L_{\mathrm{m}}}(t-t_2) \end{cases} \tag{12}$$

At this stage, the magnetic flux expression of the side column and the center column of the core are as follows:

$$\begin{cases} \Phi_{\mathrm{AC1}}(t)=\Phi_{\mathrm{AC2}}(t)=\dfrac{-nV_0-V_{\mathrm{Cr}}}{N_{\mathrm{Lr}}}(t-t_2) \\ \Phi_{\mathrm{AC3}}(t)=(\dfrac{nV_0}{N_{\mathrm{P}}}-\dfrac{V_0}{N_{\mathrm{s}}})(t-t_2) \end{cases} \tag{13}$$

4) MODE D [t_3-t_4]

At t_3, i_{Lr} and i_{Lm} are equal, the transformer primary current i_p decreases to zero, and the transformer secondary rectifier diodes D_{r1} and D_{r4} currents drop to zero and reversely cut off to achieve zero current shutdown. At this stage, the load is powered by the output capacitance. L_r, L_m, and $C_r$participate in resonance together. The expressions of V_{Cr}, i_{Lr} and i_{Lm} are as follows:

$$\begin{cases} V_{Cr}(t) = \sqrt{1+L_m/L_r}\, I_{Lr}(t_3) Z_r \sin \dfrac{\omega_r}{\sqrt{1+L_m/L_r}}(t-t_3) \\ \quad + V_{Cr}(t_3)\cos \dfrac{\omega_r}{\sqrt{1+L_m/L_r}}(t-t_3) \\ i_{Lr}(t) = i_{Lm}(t) = -V_{Cr}(t_3)\dfrac{1}{Z_r\sqrt{1+L_m/L_r}} \\ \quad \times \sin \dfrac{\omega_r}{\sqrt{1+L_m/L_r}}(t-t_3) \\ \quad + I_{Lr}(t_3)\cos \dfrac{\omega_r}{\sqrt{1+L_m/L_r}}(t-t_3) \end{cases} \tag{14}$$

At this stage, the magnetic flux expression of the side column and the center column of the core are as follows:

$$\begin{cases} \Phi_{AC1}(t) = \Phi_{AC2}(t) = \dfrac{-V_{Cr}}{N_{Lr}}(t-t_3) \\ \Phi_{AC3}(t) = 0 \end{cases} \tag{15}$$

5) MODE E [t_4-t_5]

At t_4, Q_4 is turned off, and the energy stored in the resonant inductance L_r charging the parasitic capacitance C_4 of Q_4, while the parasitic capacitance C_3discharging in the loop. Due to the buffering effect of C_3 and C_4, Q_4 turns off at zero voltage.

At this stage, the magnetic flux expression of the side column and the center column of the core are as follows:

$$\begin{cases} \Phi_{AC1}(t) = \Phi_{AC2}(t) = \dfrac{V_{AB}-V_{Cr}}{N_{Lr}}(t-t_4) \\ \Phi_{AC3}(t) = 0 \end{cases} \tag{16}$$

B. THE ESTABLISHMENT OF IM MODEL

Magnetic circuit-electric circuit dual transformation method and gyrator-capacitor analogy method are two methods for analyzing and modeling IM [21], [22]. The magnetic circuit-electric circuit dual transformation method allows the magnetic parameters in the magnetic circuit to be transformed into electrical parameters in the electric circuit for description. The physical meaning of the obtained model is clear, which facilitate for parameter design and theoretical analysis. The gyrator-capacitor analogy method uses a gyrator to simulate the winding on each magnetic columns, and a capacitance to simulate the magnetic permeance. The obtained model is simple and direct, completely reflecting the electric circuit and magnetic circuit characteristics of the magnetic components, which is suitable for the needs of simulation design.

Figures 7 to 9 shows the evolution process of the equivalent circuit. Based on the winding structure of IM in figure 2, the

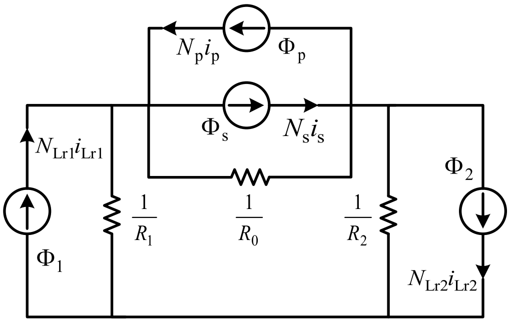

FIGURE 7. Equivalent magnetic circuit dual diagram.

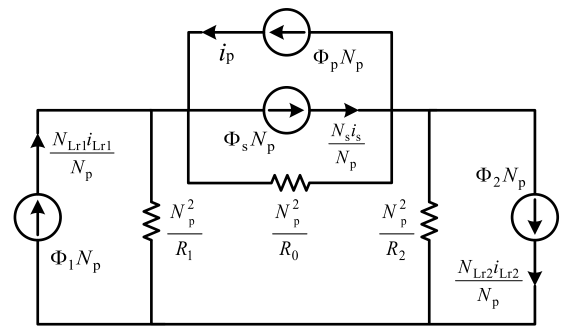

FIGURE 8. The relation diagram of flux linkage and current after scale transformation.

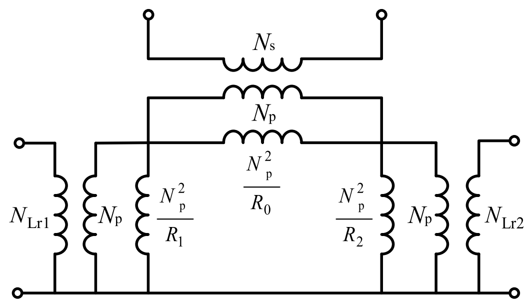

FIGURE 9. Equivalent circuit of IM.

equivalent magnetic circuit model of figure 3 is obtained. Using the duality principle to perform dual transformation on the equivalent magnetic circuit, then the equivalent magnetic circuit duality diagram of figure 7 is obtained. The flux linkage and current diagram of figure 8 is obtained by scaling transformation of the equivalent magnetic circuit dual diagram. And then to obtain the equivalent circuit diagram, as shown in figure 9, using the principle of transformer impedance transformation.

By using the gyrator-capacitor analogy method to obtain the IM gyrator-capacitor equivalent model as shown in figure 10, where C_1, C_2 and C_3 are the equivalent permeance of the two side columns and the middle column of the magnetic core respectively; C_{g1}, C_{g2} and C_{g3} are the air gap permeance of the column on both sides of the magnetic core and the center column respectively. The equivalent model can be used to link the magnetic circuit with the electric circuit structure, which provides convenience for simulation analysis.

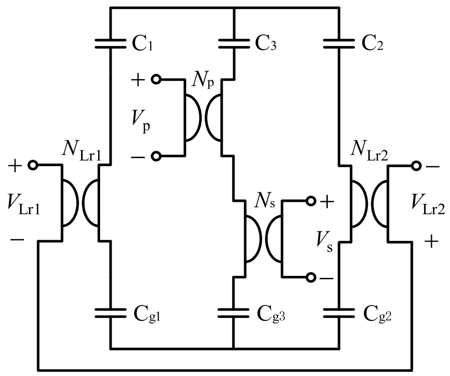

FIGURE 10. Gyrator-Capacitor equivalent model of IM.

C. DESIGN OF IM

Figure 11 shows an air gap and cross-sectional area diagram of IM, where $l_g$is the air gap length of the magnetic core (the three magnetic columns of the EE core have the same air gap to facilitate design). A_1, A_2, and A_3 are the cross-sectional areas of the two sides and the center columns of the magnetic core respectively. And due to the selection of EE-type magnetic core, $A_3 = 2A_1 = 2A_2$.

According to this, the magnetoresistance of the IM with open air gap is:

$$R_{g1} = \frac{l_g}{\mu_0 A_1}, \quad R_{g2} = \frac{l_g}{\mu_0 A_2}, \quad R_{g3} = \frac{l_g}{\mu_0 A_3}.$$

μ_0—the air permeability,which is $4\pi \times 10^{-7}$H/m.

The IM use MnZn ferrite EE40 type magnetic core, and the same air gap are opened for the three columns of the magnetic core. The specific magnetic core design parameters are shown in table 1.

When the magnetic integrated LLC resonant converter is working in mode a-c (t_0-t_3), the transformer secondary side rectifier diodes D_{r1} and D_{r4} are always conducting, so the voltage V_s of the transformer secondary winding is always

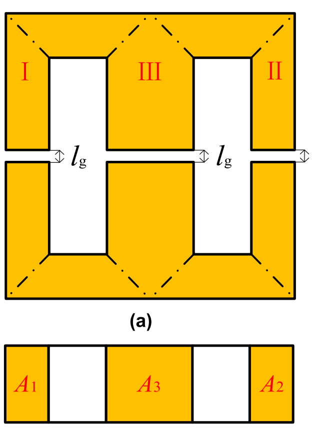

FIGURE 11. Air gap and sectional area of IM. (a) Magnetic core air gap. (b) Cross sectional area of magnetic core.

TABLE 1. The magnetic core design parameters.

Magnetic core	Magnetic column	Cross-sectional area	Air gap	Magneto-resistance
	I	64 mm^2	0.3 mm	3.730×10^6H^{-1}
EE40	III	128 mm^2	0.3 mm	1.865×10^6H^{-1}
	II	64 mm^2	0.3 mm	3.730×10^6H^{-1}

$-V_0$, and the transformer primary side voltage is clamped at nV_0. At this stage, L_r and C_r resonate together. The voltage V_s can be expressed as:

$$V_s = -V_0 = -N_s \frac{d\Phi_3}{dt} \quad (t_0 \leq t \leq t_3) \tag{17}$$

Therefore, for the magnetic column III, the magnetic flux generated by the two side columns will not circulate in the magnetic column III, that is, it has no effect on the magnetic column III, and the magnetic flux density reaches the maximum value during the period t_0 to t_3, so the maximum flux density of magnetic column III is as follows:

$$B_{3\max} = \frac{\Phi_{3\max}}{A_3} = \frac{V_0}{2A_3N_s}(t_3 - t_0) \tag{18}$$

When the magnetic integrated LLC resonant converter is working in mode a (t_0-t_1):

$$\begin{aligned} V_{Lr} &= V_{in} - V_p - V_{Cr} \\ &= N_{Lr1}\frac{d\Phi_1}{dt} + N_{Lr2}\frac{d\Phi_2}{dt} \quad (t_0 \leq t \leq t_1) \end{aligned} \tag{19}$$

At t_1, the magnetic flux density of magnetic column III reaches the maximum value, and the maximum magnetic flux density is:

$$B_{1\max} = \frac{\Phi_{1\max}}{A_1} = \frac{[V_{in} - \frac{nV_0(N_p - N_{Lr})}{N_s}](t_1 - t_0)}{A_1(N_{Lr1} + N_{Lr2})} \tag{20}$$

According to the relationship between the magnetic flux of three magnetic columns, $\Phi_2 = \Phi_1 + \Phi_3$, so the maximum flux density of magnetic column III is as follows:

$$\begin{aligned} B_{2\max} &= \frac{\Phi_{1\max} + \Phi_{3\max}}{A_2} \\ &= \frac{1}{A_2}\{\frac{[V_{in} - \frac{nV_0(N_p - N_{Lr})}{N_s}](t_1 - t_0)}{N_{Lr1} + N_{Lr2}} + \frac{V_0}{2N_s}(t_3 - t_0)\} \end{aligned} \tag{21}$$

The derivation of the above equations can be used to verify whether local magnetic columns will be saturated when designing IM, so as to optimize the magnetics design.

IV. SIMULATION OF MAGNETIC INTEGRATED LLC RESONANT CONVERTER

A. SIMULATION ANALYSIS OF GYRATOR-CAPACITOR MODEL

The gyrator-capacitor model has the advantages of convenient modeling and suitable for simulation analysis. In order

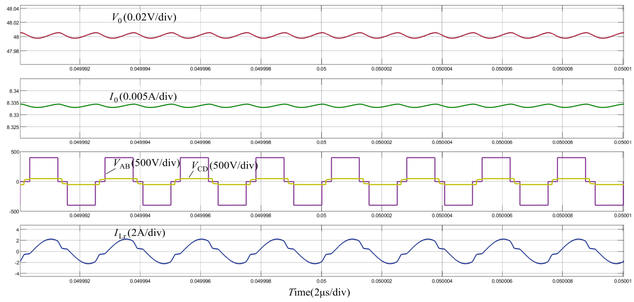

FIGURE 12. The steady-state simulation waveform under full load of DM.

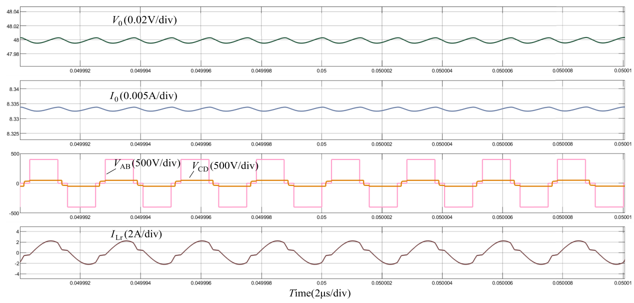

FIGURE 13. The steady-state simulation waveform under full load of IM transformer.

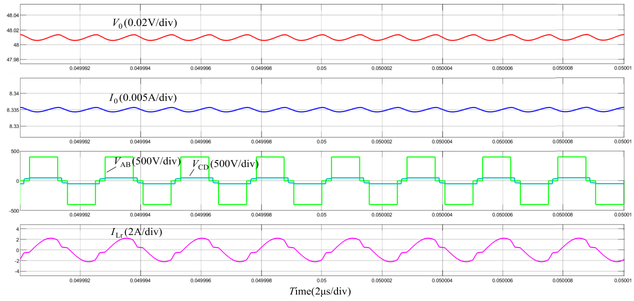

FIGURE 14. The steady-state simulation waveform under full load of IM.

to verify the performance of different magnetic components, the equivalent models of each magnetic components were established respectively. Through the co-simulation of PSpice and Simulink, the steady-state waveforms of the LLC resonant converter under DM, IM transformer, and IM are compared, and the converter transient characteristics with the IM are verified. The simulation parameters are as follows: input DC voltage $V_{in} = 360$V, output voltage $V_0 = 48$V, load current $I_0 = 8.33$A, output power P = 400W, transformer ratio $n = 8{:}1$, switching frequency $f_s = 350$kHz, the devices used in the simulation are all ideal devices. And the simulation waveforms are as follows:

Figure 12 is the steady-state simulation waveform under full load of DM, figure 13 is the steady-state simulation waveform under full load of IM transformer, and figure 14 is the steady-state simulation waveform under full load of IM. As can be seen from the above figures, in the steady state, the simulation waveforms of the voltage V_{AB} between primary

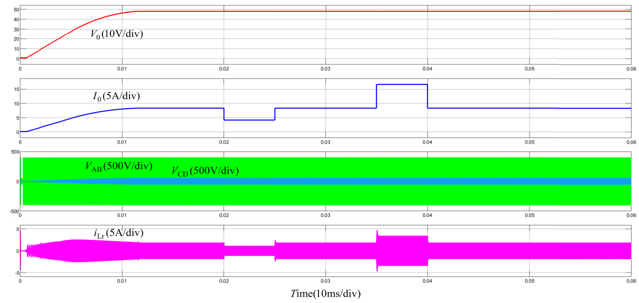

FIGURE 15. The closed-loop load switching simulation waveform of IM.

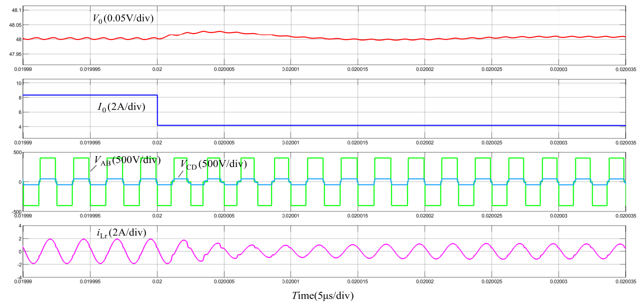

FIGURE 16. The closed-loop load switching simulation waveform of IM.

side full bridge, the secondary voltage V_{CD} of the transformer, and the resonant inductance current i_{Lr}under the two magnetic integration methods are basically the same as DM. The output voltage $V_0$and output current I_0 of the three methods all reach the rated value. Using IM and IM transformer has the same working effect as the DM, and they all conform to the basic characteristics of LLC resonant converter.

Figure 15 shows the closed-loop load switching simulation waveforms of IM. The output voltage V_0, the output current I_0, the voltage V_{AB} between primary side full bridge, the secondary voltage V_{CD} of transformer, and the resonant inductance current i_{Lr} were measured respectively. Figure 16 shows the amplification waveforms of the simulation results of figure 15 in the range of 19.99ms to 20.035ms, and the load switched from full to half at 20ms. Figure 17 shows the amplification waveforms of the simulation results of figure 15 in the range of 34.95ms to 35.25ms, and the load switched at 35ms. Figure 18 shows the further enlarged waveforms of the simulation results of figure 17 from 34.99ms to 35.05ms. It can be seen from figure 15 that during the entire simulation time period, when the load is switched, the output voltage overshoot of IM is small, the output voltage waveform is almost unaffected, the dynamic response speed of the system is fast, and the resonant current changes with the switching of the load. In figure 16, when switched from full-load to half-load at 20ms, the output voltage overshoot is small, and it quickly returns to the rated output voltage. In figure 17 and figure 18, when the load is switched at 35ms, the output voltage overshoot is slightly larger, but it can also quickly returns to the rated value. In a word, whether under the static or dynamic condition, the system of IM has the smaller output

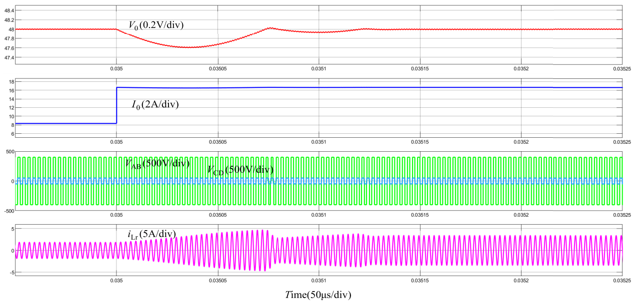

FIGURE 17. The closed-loop load switching simulation waveform of IM.

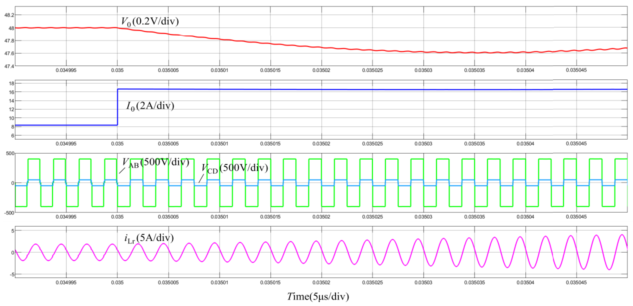

FIGURE 18. The closed-loop load switching simulation waveform of IM.

current ripple and output voltage ripple, and has fast dynamic response speed.

B. THE FINITE ELEMENT SIMULATION OF MAGNETIC COMPONENTS

In order to verify the internal magnetic flux density and magnetic field intensity distribution of different magnetic components, the finite element simulation com-parison of DM, IM transformer and IM were compared by using the ANSYS Maxwell electromagnetic simulation software. Considering the influence of temperature rise, the saturation magnetic density is about 0.35T. EE30 core is adopted as the resonant inductance of DM, the number of turns is 15, and the air gap is 0.6mm. EE35 magnetic core is adopted as the transformer of DM, the number of primary winding turns is 24, the secondary winding turns is 3, and the center column air gap is 0.2mm. The IM transformer is EE40 magnetic core, the number of primary winding turns is 16, the secondary winding turns is 2, and the air gap is 0.4mm. EE40 magnetic core is adopted for the IM, through equations (17) to (21) calculate the resonant inductance winding turns and transformer winding turns of the IM as: $N_{Lr1} = N_{Lr2} = 7$, $N_p = 16$, $N_s = 2$, and the air gap is 0.3mm.

Figure 19 is a finite element simulation of the discrete resonant inductance, and the maximum magnetic flux destiny is about 0.20T. Figure 20 is a finite element simulation of the discrete transformer, and the maximum magnetic flux destiny is about 0.29T. Figure 21 is a finite element simulation of an IM transformer with a maximum magnetic flux density about 0.27T. The maximum magnetic flux density of the

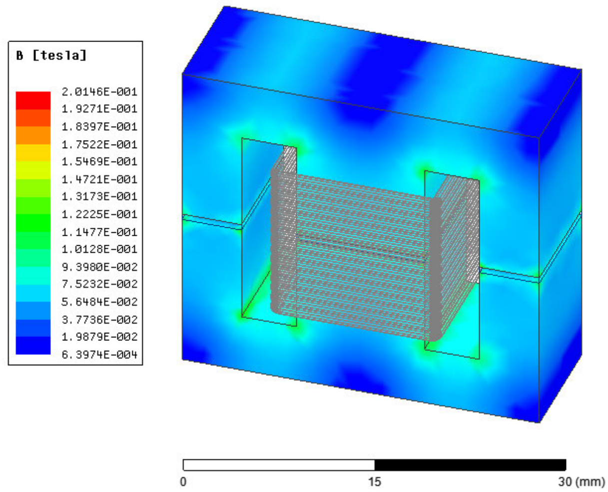

FIGURE 19. Magnetic flux density distribution of discrete resonant inductance.

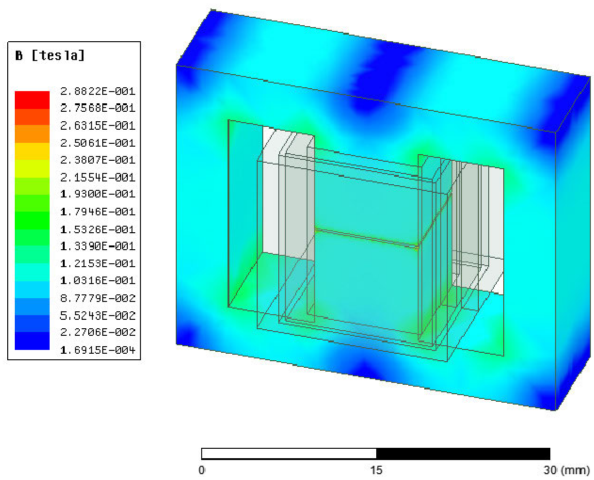

FIGURE 20. Magnetic flux density distribution of discrete transformer.

above magnetic components are all less than the saturation magnetic flux density of 0.35T, and all of them meet the normal operation requirements.

The IM simulation model was constructed in Ansys Maxwell-2D simulation environment, and the magnetic flux distribution of the IM is shown in figure 22. It can be seen that the magnetic flux of the IM is generated by the resonant inductance winding and the transformer primary winding. The magnetic flux is distributed in the two sides of columns and the center column, and a small amount of edge magnetic flux is generated at the side columns air gap, and there is less magnetic leakage. This structure achieves basically no coupling between magnetic fluxes.

The IM model was constructed in the Ansys Maxwell-3D transient simulation environment, and the external circuit magnetizing source was loaded into the model. The magnetic flux density distribution of each magnetic columns of the IM at the transient 0.016s was obtained as shown in figure 23.

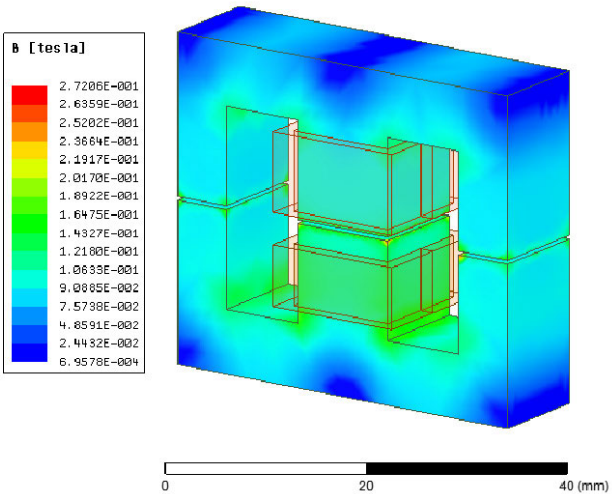

FIGURE 21. Magnetic flux density distribution of IM transformer.

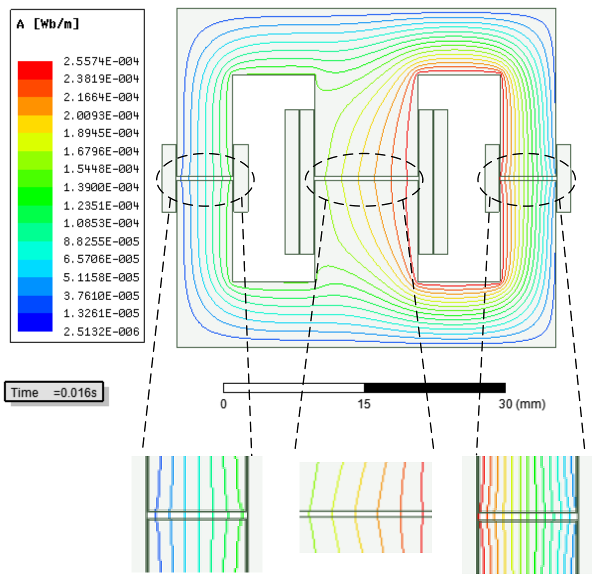

FIGURE 22. Magnetic flux distribution of IM.

It can be seen that the magnetic flux density distribution of the magnetic core is relatively uniform, and there is no phenomenon of large local magnetic flux density. The maximum magnetic flux density is about 0.24T. The magnetic core has not reach the saturated magnetic flux density of 0.35T during the whole working process, so the choice of IM magnetic core meets the design requirements of this paper.

It can be seen from figure 21 that in order to use transformer leakage inductance to provide resonant inductance, the primary winding and secondary winding of the transformer are wound up and down along the magnetic column. But, this will cause the leakage inductance of the transformer secondary side can not be fully utilized and the loss of the transformer will be increased. As the figure 23 shows, IM has lower saturation magnetic density and higher utilization of magnetic core than IM transformer. Therefore,

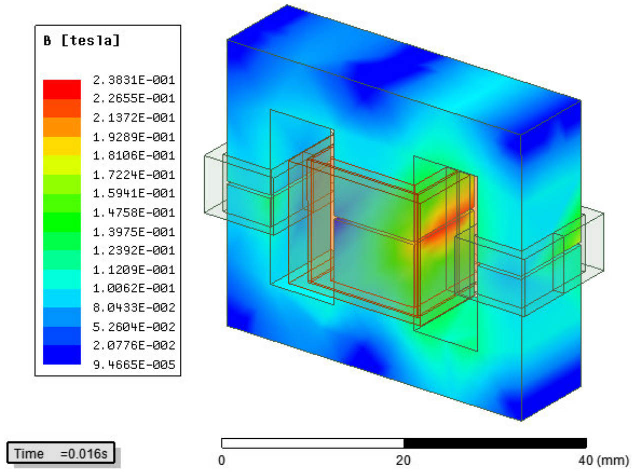

FIGURE 23. Flux density distribution of IM.

compared with IM transformer, IM can select smaller magnetic core and further reduce the volume and weight of magnetic components.

V. EXPERIMENTAL VERIFICATION

In order to verify the correctness and advantages of the IM structure design with independent inductance winding, a 400W experimental prototype is built for experiment. The parameters of the experimental prototype are shown in table 2. Compared with the LLC resonant circuit with DM, only the discrete magnetic components was replaced by the integrated magnetics, and other parameters remain unchanged. EE30 and EE35 are adopted as the DM resonant inductance and the transformer magnetic cores respectively, and EE40 is adopted as the IM magnetic cores. The DM and IM parameters are consistent with the simulation.

TABLE 2. Experimental parameters of prototype.

Parameters	Value
Switching frequency	350 kHz
Input voltage	360V
Output voltage	48 V
Load current	8.33A
Output power	400 W
Transformer ratio	8:1
Output capacitor	1000 µF
Resonant inductance	64.51 µH
Magnetizing inductance	387.1 µH
Resonant capacitance	2.45 nF
Full bridge switches	GaN-GS66508B
Rectifier diode	MBR2015DCT

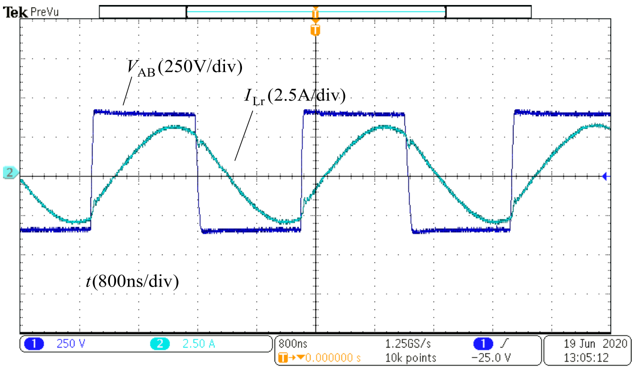

FIGURE 24. The resonant current and primary side full bridge voltage waveforms of DM.

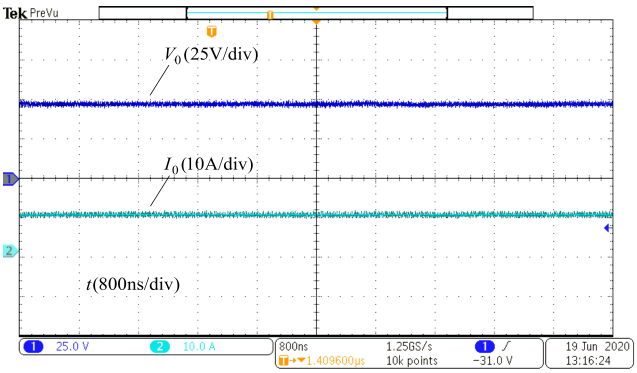

FIGURE 25. Steady-state output voltage and current waveforms of DM.

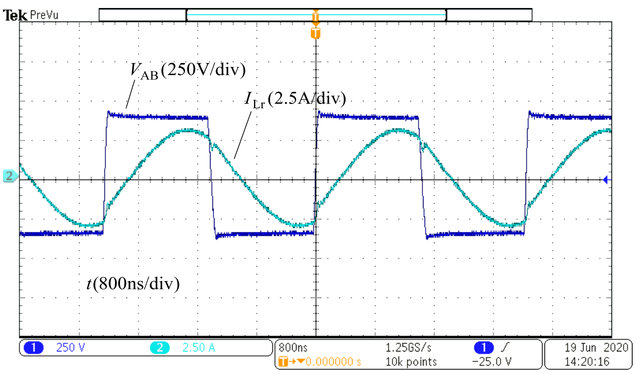

FIGURE 26. The resonant current and primary side full bridge voltage waveforms of IM.

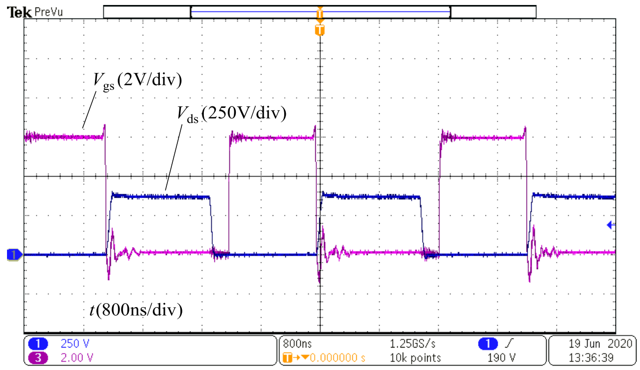

FIGURE 27. Primary side switches ZVS waveform of IM.

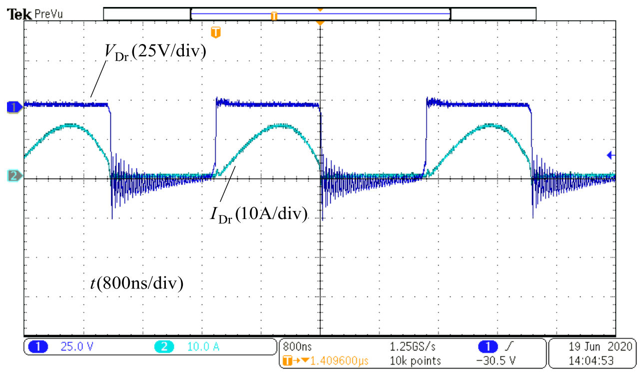

FIGURE 28. Rectifier diodes ZCS waveform of IM.

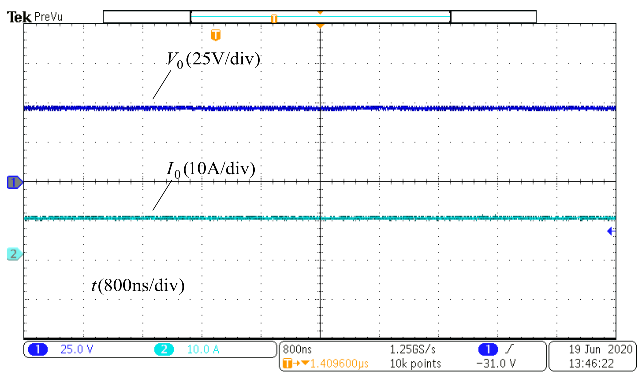

FIGURE 29. Steady-state output voltage and current waveforms of IM.

Figure 24 to 25 shows the experimental waveforms of LLC resonant converter with DM and figure 26 to 29 shows the experimental waveforms of LLC resonant converter with IM. Figure 26 is the waveform of resonant current and primary side full bridge voltage under IM, it can be seen that using the IM structure achieves the same effect as the discrete magnetic components in figure 24. It can be seen from figure 27 that after the drain-source voltage V_{ds} at both ends of the switches crosses zero, the gate-source voltage V_{gs} starts to trigger, which realizes the ZVS of the switches. From figure 28, it can be seen that when the rectifier diode voltage V_{Dr} at zero crossing, the rectifier diode current I_{Dr} is also crosses zero, which realizes the ZCS of the rectifier diode. As shown in figure 29, compared with the wave-forms under DM in figure 25, the output current ripple of the converter is small and the output voltage is stable. The above prototype test results shows that applying the magnetic integrated structure to the LLC resonant converter, the ZVS of the primary side switches and the ZCS of the secondary side rectifier diode can be realized, and also the output current ripple is small and the output voltage stable. LLC resonant converter has reached the original design intention.

Through measurement under the constant switching frequency of 350kHz, compared with DM, the volume and weight of IM are reduced by 25.68% and 43.82% respectively, which increases the power density of the converter. Under the same experimental conditions, the efficiency

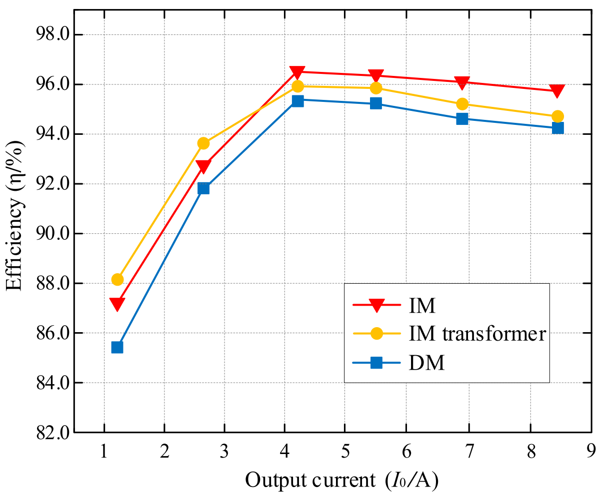

FIGURE 30. Efficiency curve.

comparison curve of the converter when using IM, IM transformer and DM can be obtained as shown in figure 30. It can be seen that the efficiency of the converter is relatively low at light load, and when the output current increases, the efficiency gradually increases. When the output current is less than 3.5A, the efficiency of IM transformer is greater than IM, but when the current is greater than 3.5A, the efficiency of IM is greater than IM transformer. It indicates that the leakage inductance of the IM transformer increases with the gradual improvement of output current, resulting in an increase in converter loss and a decrease in efficiency. And when the output current is 4.3A, all three cases reached the maximum efficiency. At this time, the efficiency of DM is 95.2%, the efficiency of IM transformer is 95.9% and the efficiency of IM is 96.3%. In summary, in full load range, the efficiency of IM and IM transformer is higher than that of DM.

VI. CONCLUSION

In this paper, a magnetic integrated LLC resonant converter with independent inductance winding was proposed. The resonant inductance and magnetizing inductance are integrated with transformer in the same core by using the decoupling integration method. After integrat-ion, the resonant inductance and the transformer do not affect each other, and the converter can achieve stable and efficient operation. Compared with the existing solution of magnetic integrated LLC resonant converter, this method can reduce the leakage inductance between the transformer windings and decrease the magnetic saturation of the integrated magnetics, thereby reducing the magnetic core loss and improving the efficiency of the converter. Through measurement under the constant switching frequency of 350kHz, compared with DM, the volume and weight of IM are reduced by 25.68% and 43.82% respectively, making the power density of the converter effectively improved and reducing the cost. Finally, an experimental prototype with switching frequency of 350kHz and output power of 400W is built. The experimental results suggest that the application of IM structure can realize the soft switching characteristics of LLC resonant converter, and verifies the correctness of the proposed method.

REFERENCES

[1] Z. Wang, Y. Zhao, J. Zhang, X. Wu, and F. Yi, "Parameter model and design of LLC half bridge resonant converter," *Trans. China Electrotech. Soc.*, vol. 27, no. 12, pp. 51–55, 2012.

[2] S. Chen, Z. Lv, and W. Yao, "Research and implementation of LLC Resonant Soft Switching DC transformer," *Trans. China Electrotech. Soc.*, vol. 27, no. 10, pp. 163–169, 2012.

[3] H.-N. Vu and W. Choi, "A novel dual full-bridge LLC resonant converter for CC and CV charges of batteries for electric vehicles," *IEEE Trans. Ind. Electron.*, vol. 65, no. 3, pp. 2212–2225, Mar. 2018.

[4] S.-Y. Chen, Z. Rong Li, and C.-L. Chen, "Analysis and design of single-stage AC/DC*LLC* resonant converter," *IEEE Trans. Ind. Electron.*, vol. 59, no. 3, pp. 1538–1544, Mar. 2012.

[5] Y. Yuan, F. Luo, and P. Hu, "A bridge type LLC resonant DC-DC converter," *Proc. CSEE*, vol. 34, no. 36, pp. 6415–6425, 2014.

[6] Q. Zhao, H. Liu, J. Yuan, and G. Cui, "Interleaving and parallel technology of full bridge LLC Resonant Converter Based on phase shifting compensation," *Trans. China Electrotech. Soc.*, vol. 33, no. 12, pp. 2777–2787, 2018.

[7] X. Wang, G. Wang, X. Sun, and D. Liu, "Control strategy of three-level half bridge LLC resonant converter with wide range of output voltage," *Trans. China Electrotech. Soc.*, vol. 32, no. 21, pp. 24–33, 2017.

[8] J. Deng, S. Li, S. Hu, C. C. Mi, and R. Ma, "Design methodology of LLC resonant converters for electric vehicle battery chargers," *IEEE Trans. Veh. Technol.*, vol. 63, no. 4, pp. 1581–1592, May 2014.

[9] Z. Lu and W. Chen, "Research on magnetic integration technology of multi-channel interleaved parallel flyback converter," *Proc. CSEE*, vol. 29, no. 18, pp. 41–46, 2009.

[10] Q. Chen, X. Ruan, and Y. Yan, "Magnetic integration technology and its application in switching power supply," *Trans. China Electrotech. Soc.*, vol. 19, no. 3, pp. 1–8, 2004.

[11] S. Gao and H. Wang, "A new approach integrated magnetics double-frequency DC/DC converter," *IEEE Access*, vol. 8, pp. 148301–148314, 2020.

[12] X. Jin, L. Wan, J. Xu, B. Qian, and Z. Lv, "Input voltage range expansion method of half bridge LLC converter based on magnetic amplifier," *Trans. China Electrotech. Soc.*, vol. 33, no. 21, pp. 5026–5035, 2018.

[13] X. Sun, Y. Shen, W. Li, and B. Wang, "Interleaving and parallel bidirectional buck / boost integrated LLC resonant three port DC converter," *Trans. China Electrotech. Soc.*, vol. 31, no. 14, pp. 165–175, 2016.

[14] H. Wu, T. Mu, X. Gao, and Y. Xing, "A secondary-side Phase-Shift-Controlled LLC resonant converter with reduced conduction loss at normal operation for hold-up time compensation application," *IEEE Trans. Power Electron.*, vol. 30, no. 10, pp. 5352–5357, Oct. 2015.

[15] Q. Chen, J. Wang, and Y. Ji, "Soft start and power reversing control of two-way LLC Resonant DC transformer," *Trans. China Electrotech. Soc.*, vol. 29, no. 8, pp. 180–186, 2014.

[16] B. Yang, R. Chen, and F. C. Lee, "Integrated magnetic for LLC resonant converter," in *Proc. APEC. 17th Annu. IEEE Appl. Power Electron. Conf. Expo.*, 2002, pp. 346–351.

[17] K. Wu, Q. Chen, K. Jin, and X. Ruan, "Integrated magnetic for hybrid full-bridge three-level LLC resonant converter," in *Proc. Int. Electri. Mach. Syst. Conf.*, 2008, pp. 1937–1941.

[18] W. Martinez, M. Noah, S. Endo, K. Nanamori, S. Kimura, Y. Itoh, M. Yamamoto, J. Imaoka, and K. Umetani, "Three-phase LLC resonant converter with integrated magnetics," in *Proc. IEEE Energy Convers. Congr. Expo. (ECCE)*, Sep. 2016, pp. 1–8.

[19] M. Li, Z. Ouyang, and M. A. E. Andersen, "High Frequency LLC Resonant Converter with Magnetic Shunt Integrated Planar Transformer," *IEEE Trans. Power Electron.*, vol. 34, no. 3, pp. 2405–2415, Mar. 2019.

[20] S. Li, Q. Min, E. Rong, R. Zhang, X. Du, and S. Lu, "A magnetic integration half-turn planar transformer and its analysis for LLC resonant DC-DC converters," *IEEE Access*, vol. 7, pp. 128408–128418, 2019.

[21] D. C. Hamill, "Lumped equivalent circuits of magnetic components: The gyrator-capacitor approach," *IEEE Trans. Power Electron.*, vol. 8, no. 2, pp. 97–103, Apr. 1993.

[22] L. Yan and B. Lehman, "A capacitor modeling method for integrated magnetic components in DC/DC converters," *IEEE Trans. Power Electron.*, vol. 20, no. 5, pp. 987–996, Sep. 2005.

SHENGWEI GAO was born in Tianjin, China, in 1978. He received the B.S., M.S., and Ph.D. degrees in electrical engineering from the Hebei University of Technology, in 2005 and 2011, respectively.

From 2005 to 2011, he was a Lecturer with the School of Electrical Engineering and Automation, Tiangong University. Since 2011, he has been an Assistant Professor with the Electrical Engineering and Automation Department, Tiangong University, where he has been a Professor, since 2020. He did his postdoctoral work with the School of Mechanical Electronics, Tiangong University, in 2019. He is the author of one book, more than 50 articles, and more than 20 inventions. His research interests include power electronic transformation technology and application, and embedded system design and application.

Dr. Gao was a recipient of the Outstanding Young Teacher Award of Tianjin, in 2011, the Sang Ma Truse Fund of Hong Kong, China, and the First Prize of Teaching Achievement of Tianjin Municipal Government, in 2019.

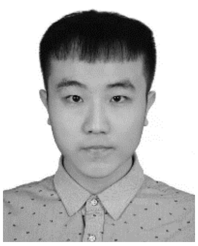

ZIYI ZHAO was born in Hebei, China, in 1996. He received the B.S. degree in electrical engineering from the City College, Hebei University of Technology, Tianjin, China, in 2019. He is currently pursuing the M.S. degree in electrical engineering with Tiangong University, Tianjin. His current research interests include power electronics transformation technology and application, and switching power supply magnetic integration technology.